Jestr

Journal of Engineering Science and Technology Review 15 (2) (2022) 54 - 60

JOURNAL OF
**Engineering Science and Technology Review**

Research Article

www.jestr.org

# Characterization of Sandstone Pore Network using Mercury Porosimetry, Helium Porosimetry and Scanning Electron Microscopy

**Paul E. Dim*** **and Sean P. Rigby**

*Department of Chemical and Environmental Engineering, University of Nottingham, University Park, Nottingham NG7 2RD, U.K.*

Received 21 June 2020; Accepted 10 June 2022

***Abstract***

Porosity and total pore volume are fundamental properties which are vital in gaining a comprehensive insight into the structure of porous rocks. Sherwood sandstone was characterized using Mercury Intrusion Porosimetry (MIP), Helium Intrusion Porosimetry (HIP) and Scanning Electron Microscopy (SEM). The total intrusion pore volume and total porosity increased after treatment. While the bulk density decreased after treatment. The total accessible porosity was higher in the treated sample (26.95 % MIP and 30.67 % HIP) when compared with the raw (7.41 % MIP and 11.06 % HIP). The total pore volume was also larger in the treated sample (0.1538 mL/g MIP and 0.231 gcm-3 HIP) when compared with the raw (0.0775 mL/g MIP and 0.116 gcm-3 HIP). The helium intrusion had a higher result than the mercury intrusion. These results suggest helium due to its small size must have penetrated smaller and finer pores in the rock samples. The modal pore size moved from 14000 to 24000 nm. These results show that treated has more micro, meso, macro and coarse pores than the raw samples. The densities of the samples determined from HIP and MIP decreased after treatment. SEM shows the difference in surface morphology and textural properties. The raw sample was homogenous and displayed a fine grain size, while the treated has loose and less dense-packed pore space distribution. These techniques provided more insight into the assessment of porous solids.

*Keywords:* Sandstone, Pore network, Porosity, Pore volume, Mercury porosimeter

## 1. Introduction

Sandstone is a sedimentary rock composed of mainly quartz (silica) grains with other range of materials which include feldspars, shaly, silts, limestone and clays or shales. Sandstones are mainly stratified in a simply superimposed pattern, or with intersecting bed. They usually begin as plant and animal debris transported in lakes and rivers, which accumulate and drop down on the floor of sea and oceans. Eventually, the sediments were buried by sand and other things. They are transformed through evaporation and cementation of sediments to form sandstone.

In most cases, they exist in a mixture of other stones like shale and carbonate. There are three significant categories of sandstone according to their different types of frameworks, namely quartz, feldspar and lithic grains. Sandstone started with single sand grains of different particle sizes, through the depositional process were buried and compressed and eventually resulted in void spaces forming between the sand grains [1, 2]. The successive depositions of sediments at the shore-line or in the form of fluvial or deltaic alluvia resulted in the formation of pore spaces of different sizes. These pores are connected with others to form a porous system; some have one entrance, and some are sealed totally from other void spaces. There are three main groups of voids found in porous solids, some are connected both ends, some have a single connection, and no connection known as sealed voids [1, 2]. The closed pores are not accessible; they terminate within the material. The interconnected through pores permit fluid flow through the material and, hence, are the most crucial pore structure characteristics of the material. The internal structure of sandstone influenced by intergranular areas are vital for understanding fluid flow or transport inside the rock [3]. Researches have shown that pore structure of porous solids can control imbibition in the pulp and paper technology field [4]. It is also responsible for diffusion [5], and fluid flow in porous media [6, 7], and thermal conductivity [8].

Mercury Intrusion Porosimetry (MIP), Scanning electron microscopy (SEM), Helium Intrusion Porosimeter (HIP), X-ray diffraction (XRD), and Transmission electron microscopy (TEM) are generally used for the analysis of porosity and pore properties of rocks and other porous material [9, 10]. It is worth noting; these methods can only probe specific pore size range, and thus cannot assess the properties of a sample independently. Therefore, in this study, HIP, MIP and SEM will be employed. More recently some studies have been reported on characterization of the pore properties of porous materials such as Silica [11], 2014), Coal [9, 12], Rock [6, 13, 14], Graphite [15], Artificial sandstone [16], Cement [17], Catalysts [18] and Alumina [19]. Mercury intrusion technique for long has been in use to characterise the textural properties of porous materials [20]. It is most useful in probing pores between about 0.003 – 400 μm size. This method can provide valuable information, that will aid the assessment of different structural properties or parameters of the solid rock. This feat is achievable only by MIP, but not without its disadvantages. Its access only pore mouth, and not the real size of the pore body. The sealed or isolated pore cannot be analyzed because there is no opening for mercury to invade the pore; the data interpretation relies on model pore geometry [21]. Furthermore, for analysis, it requires drying the small sample

*E-mail address: pevdim@yahoo.com
ISSN: 1791-2377 
doi:10.25103/jestr.152.08

before measurement, in most cases may not wholly reflect the exact properties of the sample [22].

For many decades, mercury intrusion porosimeter method has been in use for structural assessment of sandstone rocks. As mentioned earlier, mercury porosimeter cannot access any pore that is closed from outside the sample. Therefore, helium pycnometer will be employed to assess the isolated pores [23]. The biggest challenges remain the better understanding of pore distribution of heterogeneous pore network of sandstone rocks [24]. The objective of the study will be focused on using an integrated approach of Mercury Intrusion Porosimetry, Helium Intrusion Porosimeter and Scanning Electron Microscope techniques for pore structure characterisation.

## 2. Materials and Methods

The rock sample of Sherwood sandstone was obtained from the Cleethorpes number 1 borehole from a depth of about 1350 m, found in the Lincolnshire and East Yorkshire basin [25]. According to Brook et al. [26], based on location, the sandstone differs in nomenclature, is known as Bunter Sandstone, at the offshore and Sherwood Sandstone, at the onshore. All the rock samples were supplied as raw and treated, according to Hall et al. [27]. The rock core sample of dimensions 150 mm in length and 44 mm diameter, was placed in a flow cell and surrounded by a Teflon membrane. A higher-pressure confining fluid surrounded the sample such that the Teflon membrane tightly fitted the sample and ensured that the $CO_2$-rich fluid flowed through the sample. The fluid for the experiment was prepared by dissolving $CO_2$ into 0.5 M NaCl (sodium chloride) (saline) water inside a Baskerville 3 litre continuously-stirred, titanium-lined autoclave. Equilibrated $CO_2$ fluid was continuously pumped from the Baskerville through the reaction flow cell containing the rock core for a period of 3 months. After which the samples were oven-dried at 70 ºC for 48 h and then cooled to room temperature in a desiccator [27]. A rock saw machine was used to resize sandstone samples into cubes of dimension 1.5 mm x 1.5 mm x 1.5 mm for MIP analysis. The symbol used for the rock samples in this study are Raw Sandstone (RS) and Treated Sandstone (TS).

### 2.1. Mercury Intrusion Porosimetry (MIP)

Mercury intrusion Porosimetry (Auto pore IV 9500, Micromeritics, USA) performed the rock analysis. By the manufacturer's standard, calibration for the accuracy of the volume measurement and pressure transducer of the instrument is 1% of the stem volume and 0.1% of the maximum pressure. From the low-pressure analysis, evacuation of the rock samples was performed to dry the adsorbed moisture and water present in the internal structure of the sample. Subsequently, the samples were transferred to a low-pressure port to ensure that any remaining adsorbed gases and vapour was completely removed. The pressure value increased gradually step by step from 0.0035 MPa to a maximum pressure of 414MPa, which yields intrusion curve as a cumulative intruded volume against applied pressures, with an assumed mercury contact angle and surface tension of 140 º and 0.485 N $m^{-1}$ respectively [28, 29, 30]. The process followed by mercury retraction, which generates extrusion curve by gradual reduction of pressure leading to the withdrawal of fluid from the solid.

### 2.2. Helium Intrusion Porosimetry (HIP)

Accupyc II 1340 Gas Pycnometer manufactured by Micrometrics; USA measured the rock samples. Before sample measurement, the instrument performed complete purging cycles to remove any impurity and to ensure the samples were clean and dry. The principle of this method based on Boyle's Law (PV = Constant), which states that pressure decreases when a confined volume of gas is allowed to expand into a larger confining space. With known volumes of the enclosed and the expanded spaces, the size of a sample previously weighed and placed in the confined space can be determined by measuring gas pressure changes. When the system reached equilibrium, the measurement repeated three times, and the average was used [12, 31, 32, 33].

### 2.3. Scanning Electron Microscopy (SEM)

The images of rock samples as obtained from Zeiss Auriga HRSEM. Before analysis, 0.05 mg of samples were sprinkled with Au-Pd for 4 minutes using Quorum T15OT. The microscope operated with high electron tension (EHT) of 5 kV for imaging.

## 3. Results

### 3.1 Mercury Intrusion Porosimetry (MIP)

The pore size distribution for the rocks was obtained from the plot of cumulative volume against pressure, as shown in Fig. 1. The Washburn equation converted the pressure values to their corresponding pore sizes [34]. The results obtained show that at maximum pressures the distribution curve is horizontal at the top, which suggests complete pore-filling. The results from MIP measurements as presented in Tab. 1. The effective porosity, total intrusion volume and average pore size changed after treatment. Total effective porosity is 7.41 and 26.95 % for raw and treated, respectively, this suggests the presence of meso, macro and coarse pores. These values are consistent with the trend of these findings [3, 25, 27, 35, 36]. The total cumulative volume from 0.0775 changed to 0.1538 mL/g, and the porosity increased from 7.41 to 26.95 %. From Fig. 1 and Tab. 1, the cumulative total intrusion volume of treated is two times larger than the raw sample. The porosity of the treated is about four times the raw sample [37].

In Figs. 1 and 2 the total pore volume of the sample increased. This suggests a change in the capacity of the rocks to contain fluids since the whole volume of a reservoir rock comprises of non- free and free flowing fluid. This pattern also suggests that some ink-bottled pores responsible for mercury hysteresis has been dissolved on treatment. For all the pores present in the sample, the ink bottle pores, which are the pores with one connection are the most important, they are responsible for the hysteresis of mercury during a mercury porosimetry [3, 22, 37]. This behaviour is apparent, as shown in Fig. 1, the amount of entrapped mercury in the treated is smaller than mercury captured in the raw after extrusion. In summary, the shape of individual pores, from the relative position of intrusion and extrusion curves can be deduced [31].

The pore size distribution from the plot of cumulative intrusion volume against pore size (Fig. 2). The sample comprises of pore throat size range of 0.0015 - 175.16 µm. Based on the principle as operated by the instrument, mercury intrusion gives direct access to the entry pressure and the pore throat. Fig. 2 shows the distribution of pore size from the test on the rock samples. The shape of mercury intrusion showed the group of pores that participated in mercury intake, and one

pore system was observed [13]. They displayed uniform pore distribution in the range of pore size, which are relevant features [6].

According to Washburn [34], the cumulative mercury intrusion volume at a specific pressure is equal to a particular pore diameter, and this is an inverse relationship between the size of pores and pressure (Fig. 2). The difference in pore sizes of raw and treated samples, could mean that number of pores in a rock sample is affected by treatment [3, 6]. From Fig. 2, the raw and treated has uniform distribution in the range of pore size. The pattern of intrusion and extrusion curves suggests the presence of the meso, macro and coarse pores sizes. They will collectively make the provisional space, pathways and channels for storage and movement of fluid in the porous media [6, 38]

**Table 1.** Structural Properties of Samples measured by Mercury Intrusion Porosimetry

| Properties | Raw | Treated |
|---|---|---|
| Total intrusion volume (mL/g) | 0.0775 | 0.1538 |
| Total pore area ($m^2$/g) | 0.403 | 0.707 |
| Median pore diameter (volume) (nm) | 13414.4 | 25516.4 |
| Median Pore Diameter (Area) (nm) | 50.2 | 28.6 |
| Average pore diameter (4V/A) (nm) | 769.2 | 870.2 |
| Bulk density at 0.52 psia (g/mL) | 2.501 | 1.680 |
| Apparent density (g/mL) | 2.702 | 2.301 |
| Porosity (%) | 7.407 | 26.95 |

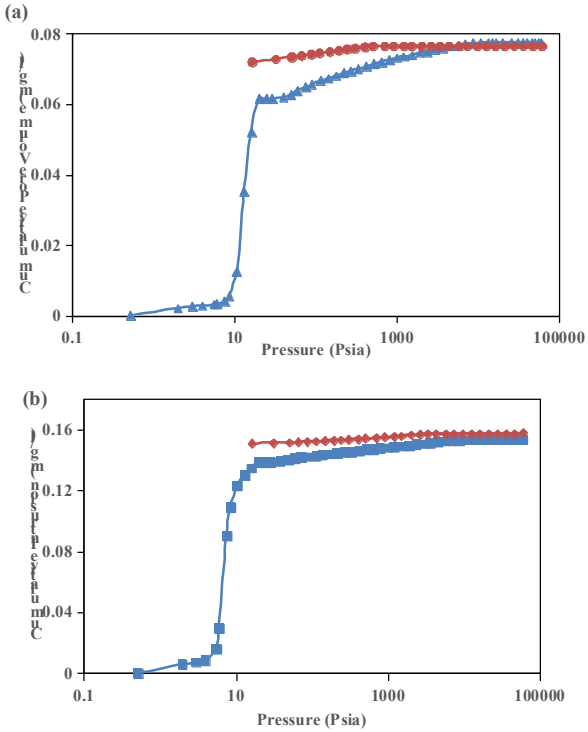


**Fig. 1.** A typical cumulative intrusion volume to pressure curve from mercury intrusion porosimeter, (a) raw sandstone with intrusion (▲) and extrusion (●) and; (b) treated sandstone with intrusion (■) and extrusion (♦).

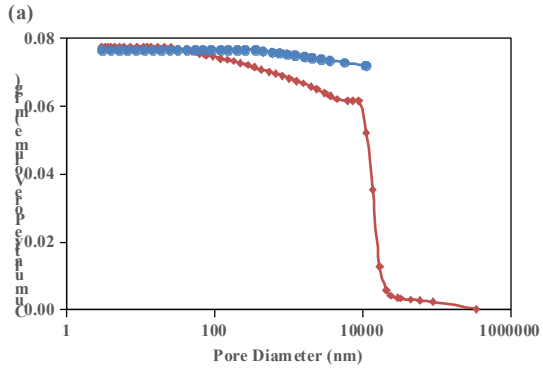


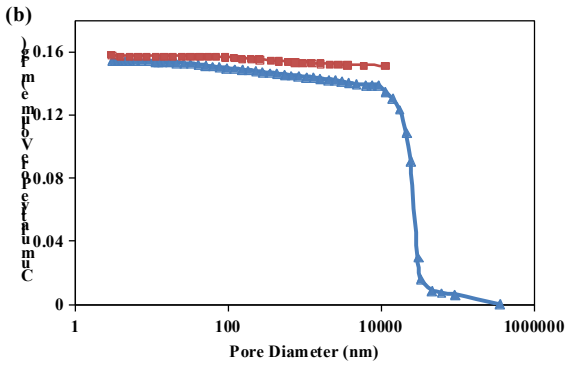


**Fig. 2.** (a) Cumulative intrusion volume to pore diameter curve from mercury intrusion porosimeter, (a) raw sandstone with intrusion (♦) and extrusion (●) and; (b) treated sandstone with intrusion (▲) and extrusion (■).

In the classification of pores, according to the International Union of Pure and Applied Chemistry (IUPAC) [39], they are grouped in sizes as micro ($d \leq 2$ nm), meso between (2 - 50 nm), and macro if the size is between 50 - 7500 nm and rough or coarse pore if the size is > 7500 nm [40, 41, 42, 43]. The pore standard as recommended by IUPAC is widely agreed for assessment of rocks and different porous materials [38, 44, 45]. Fig. 3 depicts the pore size distribution of rock samples as a function of log differential intrusion volume against pore throat. The curves can assess pore size range, modal and dominant pore size. Therefore, based on qualitative assessment the behaviour of the distribution curves as displayed by the samples is unimodal (single peak), meaning the presence of a single dominant family of pores [6].

According to Fathima et al. [8], quantitative analysis of pore size distribution curves can give information on changes in pore structure of a sample. The assessment of rock network system is essential to determine the field application for sandstone and other various rocks. As shown in Fig. 3, the comparison of pore size distributions of the raw and treated exhibited unimodal (single peak) pore size distributions of 7400 - 30000 nm and 7400 - 128000 nm. These show the presence of macropores and a higher number of coarse or rough pores. The modal pore size moved from 14000 nm to 24000 nm, and this has clearly shown the displacement of the pore to bigger diameter [4], which means a 73 % increment in modal pore diameter. The differences found between the two

samples are not only in terms of total cumulative volume but also the range of pore size distribution, as shown in Fig. 3. The average pore size diameter for raw is 769.2 nm (0.769 µm); for treated, the average pore size diameter is 870.2 nm (0.870 µm) (Table 1). Generally, in pore analysis, the average pore diameter is commonly used as a representative parameter of the material [6].

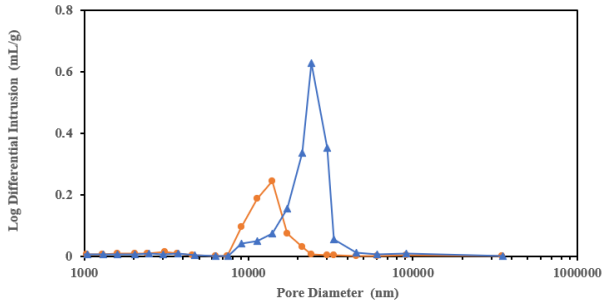


**Fig. 3.** The pore size distribution of raw sandstone (●) and treated sandstone (▲) sample.

Fig. 4 show the cumulative pore area against pore size. The total pore area for the raw and treated is 0.4029 and 0.7071 $m^{-2}g$, respectively. These represent a 76 % change in the pore area. For comparison, the plots were superimposed. Both samples displayed similar characteristics in phase 1 of the plots in the pore size range of approximately 62 - 10000 nm. While in phase 2 of the intrusion curve which occurred in the pore size range of 3 - 62 nm, this is substantially mesoporous change. It has displayed different pore properties such as pore wall coarseness and roughness. A transition point where the two curves diverged at a transition pore throat of about 62 nm. The effect of treatment on the pore area increased significantly in pore size less than equal to 62 nm, suggesting the additional micro and mesoporosity.

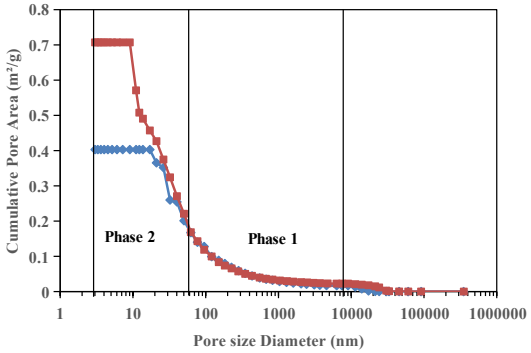


**Fig. 4.** Mercury intrusion curve of cumulative pore area as a function of pore diameter of raw sandstone (♦) and treated sandstone sample (■).

### 3.2. Helium intrusion porosimeter

Measurements were performed by gas pycnometer basically to complement the results derived from MIP. Total porosity is 11.36 and 30.57 % for raw and treated respectively. This suggests the presence of micro and mesopores [35]. The total pore volume of raw and treated are 0.116 and 0.231 $cm^3$. The comparison of porosity and pore volume, from MIP and HIP method, showed an increase after treatment, the trend indicates that the values from the HIP were higher than MIP (Fig. 5), this is because helium penetrate smaller pores that are not accessible by mercury [9]. As seen in Tab. 2, the bulk and skeletal density decreased after treatment. In other words, bulk density decreased while porosity increased; this suggests that treatment resulted in the difference in the pore structure, due to the formation of more open and connected pores. A low bulk density of rock sample could also suggest high porosity as a result of the creation of open pores by treatment. The density of the samples from HIP and MIP decreased after treatment. Therefore, a relationship between bulk density and porosity is indirectly proportional.

**Table 2** Structural properties of samples measured by Helium intrusion porosimetry

| Samples | Raw | Treated |
|---|---|---|
| Skeletal Density g/$cm^3$ | 2.17 | 1.65 |
| Pore volume $cm^3$ | 0.116 | 0.231 |
| Porosity ϕ (%) | 11.06 | 30.67 |

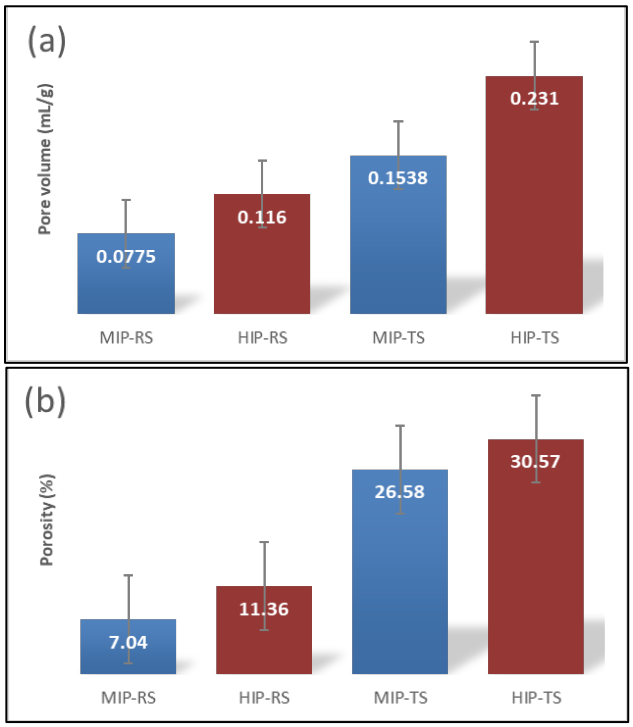


**Fig. 5.** The comparison of (a) pore volume and (b) porosity of the samples from MIP and HIP (MIP = Mercury Intrusion Porosimetry, HIP = Helium Intrusion Porosimetry, RS = Raw Sandstone, TS = Treated Sandstone).

### 3.3. Scanning Electron Microscopy (SEM)

The SEM images of the raw and treated rock sample, as shown in Fig. 6, show that the surface morphology has changed after treatment. The untreated sample showed a uniform, dense, compact surface morphology. While the treated sample exhibited a loose coarse and less thick surface structure, and this suggests that the treatment affected the pore structure. The surface structure of the samples revealed changes in pore sizes.

Generally, it is a known fact that coarse surface can increase the surface area of the rock internally (Fig. 6). The degree of orientation, arrangement and size of pores are apparent in the SEM tomography images. The raw sample showed homogeneous and fine-grain size than the treated. The morphology clearly shows the difference between the untreated and treated rock samples, especially in terms of surface smoothness and roughness.

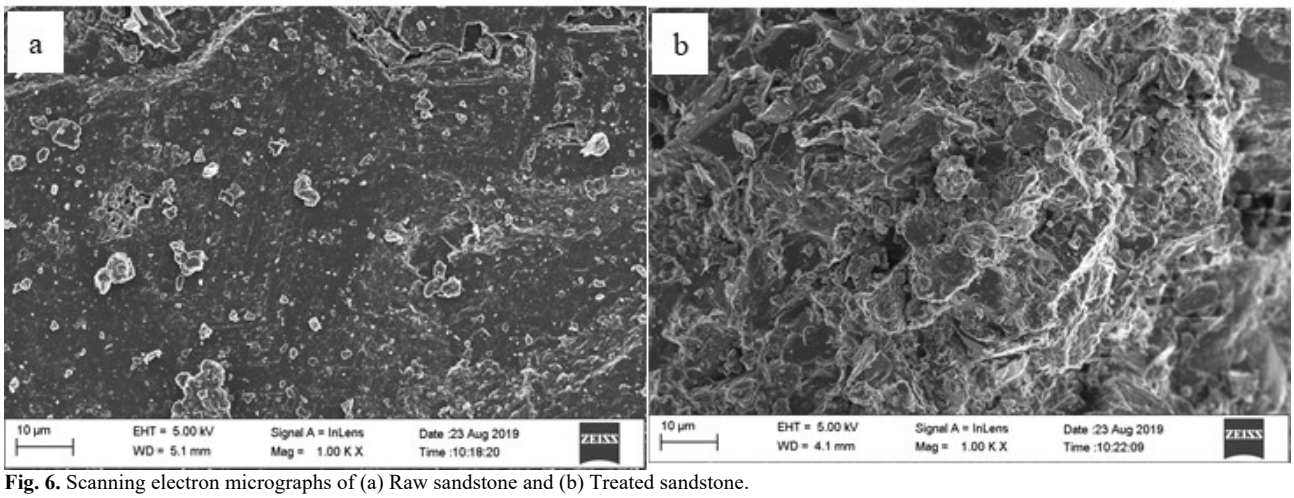


**Fig. 6.** Scanning electron micrographs of (a) Raw sandstone and (b) Treated sandstone.

## 4. Discussion of Results

Reservoir rock characterization provides critical information for system design and control, fluid estimation, creation of reservoir simulation model, prediction of reservoir production and performance, and lifespan performance optimization. Rock sample is subjected to a high pressure in the mercury porosimetry procedure. Figs. 1 and 2 show the relationship between the volume of mercury injected and the external pressure. The overall pore volume of the sample increased following treatment, as seen in Figs. 1 and 2. For the raw and treated samples, the total mercury volume peaked at 0.0775 and 0.1538 mL/g, respectively. For the treated sample, the pore volume is twice that of the raw sample. The porosity is about four times the raw sample [37]. In general, pore size and total pore volume with the same pore size are inversely proportional [3, 25, 27, 35, 36]. The existence of meso, macro, and coarse pores sizes is shown by the pattern of intrusion and extrusion curves. They will work together to create temporary space, routes, and channels for fluid storage and flow in porous medium [6, 38]. The curves in Fig. 3 can be used to determine the pore size range, modal, and dominating pore size. The samples are unimodal, indicating they contain the same family of pores, according to qualitative analysis [6]. The total pore area of the raw and treated samples is 0.4029 and 0.7071 m-2g, respectively, as shown in Fig. 4. In pore sizes less than 62 nm, the effect of treatment on the pore area increased significantly, indicating the presence of additional micro and mesoporosity. The results of the measurement with the gas pycnometer are shown in Fig. 5 and Table 2. The porosity and pore volume, as measured by the HIP technique, increased following treatment, although the mass and skeletal density decreased [9]. Increased porosity and decreased density result from the creation of more open and linked pores. This suggests that micro and mesopores are present [35]. The surface morphology of the raw and treated rock samples is shown in Figure 6. As shown in Fig. 6a, the surface of the raw rock sample was homogenous and smooth, with regular pores. The pore size distribution of the treated rock sample is exceedingly heterogeneous, rough, coarse, and uneven along macroscopic length, as seen in Fig. 6 (b). The morphology's surface smoothness and roughness were clearly different after treatment (Fig. 6 a & b). SEM scans of raw and treated samples revealed two-dimensional pore level pictures. The homogeneous and heterogeneous broad spatial distribution of distinct fractions of the pore size distribution is established using a combination of mercury intrusion porosimeter, helium intrusion porosimeter, and SEM techniques.

## 5. Conclusion

The scanning electron microscopy, mercury and helium porosimeter were employed to analyze the pores size distribution of rock samples. Total accessible porosity from MIP is 7.41, and 26.95 % and HIP was 11.06 and 30.67 % for raw and treated, respectively, this potentially suggests the presence of meso and macropores. The total cumulative volume increased after treatment from 0.0775 to 0.1538 mL/g and 0.116 to 0.231 $gcm^{-3}$ for MIP and HIP. The modal pore size increased from 14000 to 24000 nm, and this suggests a change in pore arrangement of the rock matrix. The results showed porosity and pore volume increased after treatment. Quantitatively this suggests increase in the capacity of the rocks to contain fluids. The combined technique represents a direct determination of both the closed and open pores in the sample. However, the values of structural properties obtained from the HIP were higher compare to MIP. The combination of these techniques has been used successfully for the quantitative and qualitative assessment of pore structure characteristics of the rock.



## References

1. A. Y. Dandekar, Petroleum Reservoir Rock and Fluid Properties, Taylor and Francis, Boca Raton, Florida p 13-26 (2006).
2. N. Ezekwe, Petroleum Reservoir Engineering Practice, 1Edn, Prentice Hall, USA p 65- 85 (2010).
3. K. Kovarova, R. Sevcik and Z. Weishauptova, Comparison of mercury porosimetry and x-ray microtomography for porosity study of sandstones. *Acta Geodynamica,* 9**,** 541-549 (2012).

4. M.J. Moura, P.J. Ferreira and M.M. Figueiredo, The use of Mercury Intrusion Porosimetry to the Characterisation of Eucalyptus Wood, Pulp and Paper, *O Papel*, num 6, pp. 77-79 (2002).
5. Z. Gao, Q. Hu and H. Liang, Gas diffusivity in porous media: Determination by mercury intrusion porosimetry and correlation to porosity and permeability. *Journal of Porous Media,* 16**,** 607-617 (2013).
6. A. Rahmouni, A. Boulanouar, M. Boukalouch, Y. Géraud, A. Samaouali, M. Harnafi and J. Sebbani, Relationships between porosity and permeability of calcarenite rocks based on laboratory measurements, *J. Mater. Environ. Sci*. 5 (3) 931-936 (2014)
7. Y. Zhang, B. Yang, Z. Yang and Y. Guang, Ink-bottle Effect and Pore Size Distribution of Cementitious Materials Identified by Pressurization–Depressurization Cycling Mercury Intrusion Porosimetry, Materials*,* 12, 145-155 (2019)
8. N.N. Fathima, A. Dhathathreyan and T. Ramasami, Mercury Intrusion Porosimetry, Nitrogen Adsorption, and SEM Analysis of Pores in Skin, *Biomacromolecules,* 3, 899 – 904 (2002).
9. G.N. Okolo, R.C. Everson, H.W.J.P. Neomagus, M.J. Roberts and R. Sakurovs, Comparing the porosity and surface areas of coal as measured by gas adsorption, mercury intrusion and SAXS techniques, *Fuel,* 141, 293 – 304 (2015).
10. T.F. Rexer, E.J. Mathia, A.C. Aplin and K.M. Thomas, High-pressure adsorption and characterisation of pores in Posidonia shales and isolated kerogens. *Energy Fuels,* 28: (5):2886–901 (2014).
11. B. Bafarawa, A. Nepryahin, L. Ji, E.M. Holt, J. Wang and S.P Rigby, Combining mercury thermoporometry with integrated gas sorption and mercury porosimetry to improve the accuracy of pore-size distributions for disordered solids. *Journal of Colloid and Interface Science,* 426**,** 72-79 (2014).
12. Z. Chen, T. Bai and Z. Pan, Coal Reservoir Characterization, Coal Production and Processing Technology, Taylor & Francis Group, Florida p 79-100 (2016).
13. J.A. Jarzyna, P.I. Krakowska, E. Puskarczyk and R. Semyrka, Rock Reservoir Properties from the Comprehensive Interpretation of Nuclear Magnetic Resonance and Mercury Injection Porosimetry Laboratory Results, *Appl Magn Reson* (2015) 46, 95–115 (2015).
14. L. Kong, M. Ostadhassan, C. Li and N. Tamimi, Pore characterisation of 3D-printed gypsum rocks: a comprehensive approach, *J Mater Sci*, 53, 5063–5078 (2018).
15. K.L. Jones, G.P. Matthews and G.M. Laudone, The effect of irradiation and radiolytic oxidation on the porous space of Gilsocarbon nuclear graphite measured with mercury porosimetry and helium pycnometry, *Carbon,*doi: https://doi.org/10.1016/j.carbon.2019.11.084. (2020).
16. H. Dong, H. Zhang, Y. Zuo, P. Gao and G. Ye, Relationship between the Size of the Samples and the Interpretation of the Mercury Intrusion Results of an Artificial Sandstone, *Materials,* 11, 201-212 (2018).
17. X. Wang, Y. Peng, J. Wang and Q. Zeng, Pore Structure Damages in Cement-Based Materials by Mercury Intrusion: A Non-Destructive Assessment by X-Ray Computed Tomography, Materials, 12, 22-29 (2019).
18. P.E. Dim, R.S. Fletcher and S.P. Rigby, Improving the accuracy of catalyst pore size distributions from mercury porosimetry using mercury thermoporometry. *Chemical Engineering Science,* 140, 291-298 (2016).
19. E. P. Sobina, Development of Alumina-Based Porosity Reference Materials for the Mercury Porosimetry Method. In: Medvedevskikh S., Kremleva, O. Vasil'eva I., Sobina E. (eds) Reference Materials in Measurementand Technology. RMMT, 2020. Springer, Cham. https://doi.org/10.1007/978-3-030-32534-3_10
20. D. Julve, J. Ramos, J. Pérez and M. Menéndez, Analysis of mercury porosimetry curves of precipitated silica, as an example of compressible porous solids, *Journal of Non-Crystalline Solids,* 357 ,1319 – 1327 (2011).
21. H. Giesche, Mercury Porosimetry: A General (Practical) Overview, *Part. Syst. Characterisation* , 23, 9–19 (2006).
22. J. Kaufmann, Pore space analysis of cement-based materials by combined Nitrogen sorption –Wood's metal impregnation and multi-cycle mercury intrusion, *Cement & Concrete Composites,* 32, 514–522 (2010).
23. D. Markl, A. Strobel, R. Schlossnikj, J. Bøtker, P. Bawuah, C. Ridgway, J. Rantanen, T. Rades, P. Gane, K. Peiponen and J.A. Zeitler, Characterisation of Pore Structures of Pharmaceutical Tablets: A Review, *Chemical Engineering Research and Design,* 45, 4064-4079 (2018).
24. U. Kuila, and M. Prasad, Specific surface area and pore-size distribution in clays and shales, *Geophysical Prospecting,* 61, 341–362 (2013).
25. R. Downing, D. Allen, M. Bird, I. Gale, R. Kay and F. Smith, Investigation of the geothermal potential of the UK: Cleethorpes No 1 geothermal well – a preliminary assessment of the resource, British Geological Survey, Keyworth, UK (1985).
26. M. Brook, K. Shaw, C. Vincent and S. Holloway, Gestco case study 2a-1: Storage Potential of the Bunter Sandstone in the UK sector of the southern North Sea and the adjacent onshore area of Eastern England, Sustainable Energy and Geophysical Surveys Programme Commissioned Report CR/03/154N, British Geological Survey (2003)..
27. M.R. Hall, S.P. Rigby, P.E. Dim, K. Bateman, S.J. Mackintosh and C.A. Rochelle, Post $CO_2$ injection alteration of the pore network and intrinsic permeability tensor for a Permo-Triassic sandstone. *Geofluids,* 1-15 (2015).
28. P.A. Webb, An introduction to the physical characterisation of materials by mercury intrusion porosimetry with emphasis on reduction and presentation of experimental data. Norcross (Georgia): Micromeritics Instrument Corporation, p. 1–23 (2001).
29. S.P. Rigby, P.I. Chigada, J. Wang, S.K. Wilkinson, H. Bateman, B. Al-Duri, J. Wood, S. Bakalis and T. Miri, Improving the interpretation of mercury porosimetry data using computerised X-ray tomography and mean-field DFT. *Chemical Engineering Science,* 66**,** 2328-2339 (2011).
30. J. Rouquerol, G.V. Baron, R. Denoyel, H. Giesche, J. Groen, P. Klobes, P. Levitz, A.V. Neimark, S. Rigby, R. Skudas, K. Sing, M. Thommes and K. Unge, The characterisation of macroporous solids: An overview of the methodology, *Microporous and Mesoporous Materials,* 154, 2–6 (2012).
31. S. Lowell, J.E. Shields, M.A. Thomas and M. Thommes, Density Measurement, in characterisation of porous solids and powders: Surface area, Pore size and density, Particle Technology Series. Springer Netherlands, Dordrecht, pp.326–338 (2004).
32. P. Massarotto, S.D. Golding, J.S. Bae, R. Iyer and V. Rudolph, Changes in reservoir properties from injection of supercritical $CO_2$ into coal seams-a laboratory study. *Int. J. Coal Geol*. 82, 269–279 (2010).
33. G.M. Laudone, C.M. Gribble and G.P. Matthews, Characterisation of the porous structure of Gilsocarbon graphite using pycnometry, cyclic porosimetry and void-network modelling Carbon, 73, 61 –70 (2014).
34. E.W. Washburn, The dynamics of capillary flow. *Physical Review,* 17, 273–283 (1921).
35. J.K. Pearce, G.K.W. Dawson, T.P. Blach, J. Bahadur, Y.B. Melnichenko, and S.D. Golding, Impure $CO_2$ reaction of feldspar, clay, and organic matter rich cap-rocks: Decreases in the fraction of accessible mesopores measured by SANS, *International Journal of Coal Geology* 185, 79–90 (2018).
36. J.R. Schopper, Porosity and permeability. In: Hellwege, K.-H. (Ed.), Landolt-Bornstein Numerical Data and Functional Relationships in Science and Technology, New Series, Group V. Geophysics and Space Research, vol. 1, Physical Properties of Rocks, sub vol. A. Springer-Verlag, Berlin, p. 123 – 145 (1982).
37. K.H. Hellmuth, M. Siitari-Kauppi, P. Klobes, K. Meyer and J. Goebbels, Imaging and analysing rock porosity by autoradiography and Hg-porosimetry/X-ray computer tomography-applications. *Physics and Chemistry of the Earth Part a-Solid Earth and Geodesy,* 24**,** 569-573 (1999).
38. C.R. Clarkson, N. Solano, R.M. Bustin, A.M.M. Bustin, G.R.L. Chalmers, L. He, Y.B. Melnichenko, A.P. Radliński, and T.P. Blach, Pore structure characterisation of North American shale gas reservoirs using USANS/SANS, gas adsorption, and MIP. *Fuel*, 103, 606−616 (2013).
39. International Union of Pure and Applied Chemistry (IUPAC), Manuals of Symbols and Terminology for Physico Chemical Quantities and Units. Butterwort, London, U.K p 25 – 35 (1972).
40. U. Mann, T. Hantschel, R.G. Schaefer, B. Krooss, D. Leythaeuser and R. Little, Petroleum migration: mechanisms, pathways, efficiencies and numerical simulations. In: Welte, D.H., Horsfield, B., Baker, D. (Eds.), Petroleum and Basin Evolution. Springer-Verlag, Berlin, p 340 -352 (1977).
41. K.S.W. Sing, D.H. Everett, R.A.W. Haul, L. Moscou, R.A. Pierotti, J. Rouquerol and T. Siemieniewska, Reporting physisorption data for gas/solid systems with special reference to the determination of surface area and porosity, *Pure Appl. Chem*. 57, 603−619 (1985).

42. J. Mays, A new classification of pore sizes, Studies in Surface Science and Catalysis 160, P.L. Llewellyn, F. Rodriquez-Reinoso, J. Rouqerol and N. Seaton (Editors), p 9 (2007) Elsevier BV.
43. J.H. Schon, Physical Properties of Rocks, A Workbook, Handbook of Petroleum Exploration and Production, 8, Elsevier The Boulevard, Langford Lane, Kidlington, Oxford, OX5 1GB, UK, Radarweg 29, PO. Box 211, 1000 AE Amsterdam, The Netherlands, p 67 – 77 (2011).
44. R. Bustin, A. Bustin, A. Cui, D. Ross and V. Pathi, Impact of shale properties on pore structure and storage characteristics. Proceedings of the SPE Shale Gas Production Conference; Fort Worth, TX, pp. 16−18, (2008).
45. C. Clarkson, J. Wood and S. Burgis, Nanopore-structure analysis and permeability predictions for a tight gas siltstone reservoir by use of low-pressure adsorption and mercury-intrusion techniques, *Reservoir Eval. Eng*., 15, 648−661 (2012).